Advanced low-noise aircraft configurations and their assessment: past, present, and future

CEAS Aeronautical Journal manuscript No.
(will be inserted by the editor)

Aircraft Noise Generation and Assessment

Advanced Low Noise Aircraft Configurations and Their Assessment - Past, Present and Future

Z. S. Spakovszky

October 1, 2018

Abstract Aircraft noise remains *the* key inhibitor of the growth of air transportation but the focus of the noise mitigation strategies has changed. As the propulsor fan pressure ratio (FPR) is decreased and bypass ratio (BPR) is increased for improved fuel burn and reduced environmental impact, the propulsion system noise is reduced near or even below the noise level of the airframe. Jet noise has become less of a concern and, during approach and landing, the acoustic signature is predominantly set by the airframe. Novel aircraft concepts and architectures, enabled by distributed, more integrated, and boundary layer ingesting propulsion systems, pose new aero-acoustic problems which require innovative approaches and call for teaming and collaboration as the technological challenges cut across disciplines. One past example of such a collaborative research effort was the Silent Aircraft Initiative (SAI), aimed at the conceptual design of an aircraft imperceptible to the human ear outside the airport perimeter. The initiative brought together researchers from academia, industry and government agencies. This chapter gives a brief summary of the Silent Aircraft Initiative, the SAX-40 aircraft design, and the noise reduction technologies which were pursued. A decade past SAI, novel aircraft architectures such as the D8 double bubble aircraft, the outcome of a joint effort between MIT, Aurora Flight Sciences and Pratt & Whitney, are being pursued in the quest of reducing the climate impact of aviation. With regulations continuing to reduce the allowable aviation noise emission levels, both new challenges and new opportunities are emerging. Electric, hybrid, and turbo-electric aircraft concepts are currently being investigated as potential game-changers. Independent of the level of electrification, noise will remain a major issue as air transportation is growing and mobility might become a key driver. The chapter discusses a selection of enabling technologies and their implications on acoustics and noise and gives a perspective on future trends and new directions in aero-acoustics required to address the challenges.

Keywords aircraft noise · advanced concepts · turbomachinery noise · shielding · boundary layer ingestion

Z. S. Spakovszky
Gas Turbine Laboratory, Massachusetts Institute of Technology, Cambridge MA, 02139
E-mail: zolti@mit.edu

1 The Silent Aircraft Initiative

Aircraft noise remains a major barrier in the expansion of airport operations and new regulations continue to limit noise emissions. Figure 1 indicates the downward trend in aircraft noise over time [1]. Further reductions in aircraft noise, however, become harder to achieve, and the problem is made more difficult by the anticipated increase in noise due to the growth in aircraft operations. Addressing aircraft noise has been a long-standing objective of industry, academia and

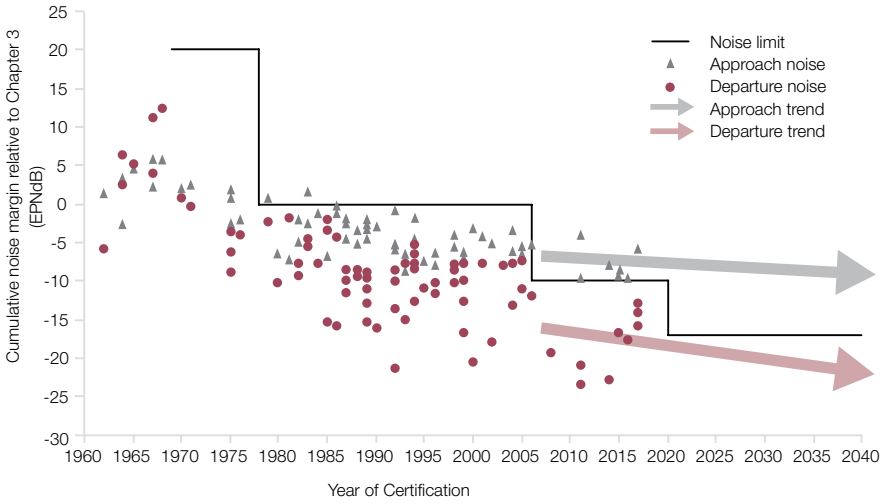

Fig. 1 Progress in aircraft noise reduction [1].

government agencies. Thomas et al. [2] give an excellent chronological summary of the relevant efforts, which has been briefly reproduced here. NASA launched the Quiet Aircraft Technology (QAT) project in 1999 working toward a mid-term 30 EPNdB cumulative goal and a far-term 60 EPNdB cumulative noise reduction goal relative to the 1997 best-in-fleet. In 2002, funded by the Propulsion Airframe Aeroacoustics (PAA) team at NASA Langley Research Center, MIT began to study an aircraft concept designed from first-principles to be functionally-silent [3]. The goal was set to reduce aircraft noise below the noise of a well-populated area. This led to a hybrid wing body (HWB) aircraft concept with aerodynamically clean lifting surfaces capable of very low approach velocity and a steep glide slope to reduce airframe noise. A distributed propulsion system with an effective bypass ratio of 20, either through multiple small engines or multiple fans driven by a common core, was proposed to reduce propulsion system noise. Integration of the propulsion system with the airframe used a "hidden" trailing edge with performance and noise benefits due to boundary layer ingestion and a high aspect ratio rectangular nozzle. In addition, an engine air-brake was proposed to dissipate the potential energy of the aircraft during descent and approach by operating the engine in wind mill mode through variable pitch fan blades. NASA also identified the hybrid wing body aircraft as the most promising advanced aircraft concept for low noise and a pathfinding study began in 2003. A summary of the NASA low noise HWB strategy and review of previous studies at that time can be found in [2]. Other low-noise aircraft configuration currently being pursued are advanced tube-and-wing type aircraft architectures, such as discussed for example in [4,5].

A related and much more comprehensive study, funded by the Cambridge-MIT Institute (CMI), was launched in 2003 dubbed the Silent Aircraft Initiative (SAI) [6]. The approach was to set the objective of a radical reduction in noise as a primary design criterion, with a specific project goal of providing a conceptual design of an aircraft quiet enough to be imperceptible to people in the urban environment around airports while being competitive with existing and next generation aircraft in terms of fuel burn and emissions. A key project outcome was the conceptual Silent Aircraft eXperimental design SAX-40, which had an estimated noise level less than the background noise of a well-populated area and a predicted 23% fuel burn reduction compared to the best of current civil aircraft.

A number of noise reduction targets have been set by the aviation industry, but SAI aimed at a major step beyond these. This stretch goal called for a highly integrated airframe and engines as well as for operations and design optimized together for low noise. This implyed that the capabilities of a range of partners (in academia, industry, and government) would be needed. From the beginning, therefore, the project was viewed as involving collaboration among organizations and among individuals with different skills (and interests).

SAI was one of the CMI Knowledge Integration Communities (KICs), research communities exploring new ways for academia, industry, and government to work together. The role of the KIC was to foster linkages and two-way flows of information between academic researchers and their colleagues in commerce to enhance the impact of the research. The SAI community comprised airframers, engine manufacturers, airport and airline operators, air traffic controllers, regulators and measurement specialists at over thirty partners, in addition to the academics.

2 Features of the Silent Aircraft Design

The target aircraft mission was set to 215 passengers with a range of 5000 nm at a cruise Mach number of 0.8. The conceptual design, depicted in Figure 2, has an airframe that differs radically from current civil aircraft. There are conventional supercritical wings but the fuselage is a lifting

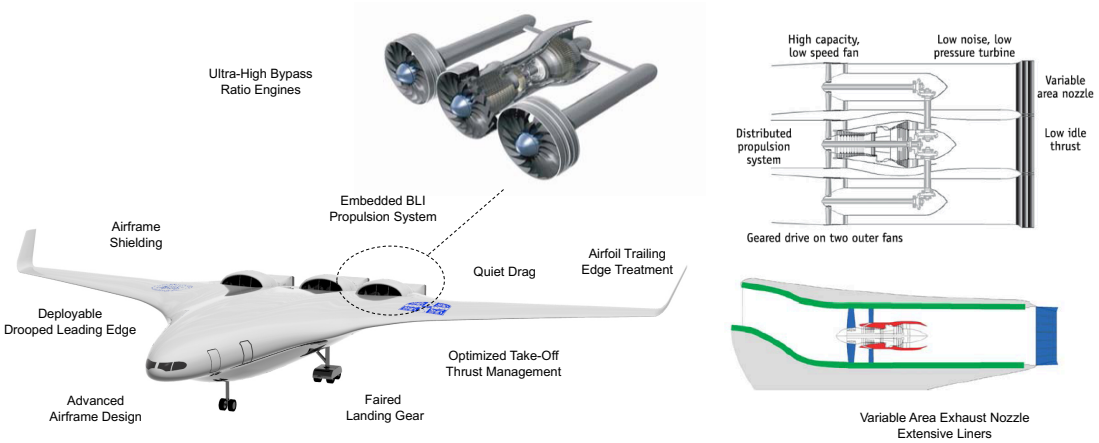

Fig. 2 The Silent Aircraft eXperimental design SAX-40 with boundary layer ingesting, embedded distributed propulsion system and lifting fuselage (left). Engine cluster comprised of turbofan and two geared auxiliary fans (right).

body aerodynamically shaped to achieve enhanced low speed and cruise performance without the need for flaps and a tail. The design parameter Mach number times lift/drag ratio (ML/D) is 20. The wing span is 222 feet (67.5 m) including the winglet, and the maximum take-off weight is 332,000 lbs (151,000 kg).

The aircraft is propelled by a distributed high bypass ratio propulsion system (cruise bypass ratio of 12) embedded in the fuselage. There are nine geared fans driven by three gas generators. Each inlet shown in Figure 2 thus feeds air to one engine cluster comprised of a turbofan and two auxiliary fans. A top view of the engines indicates the gearing for the cluster (of three fans/one engine) that sits in each of the three intakes. The side view of the engine in the duct illustrates the length of duct available for acoustic liners. The overall conceptual design was aimed at the 2030 time frame, but part of the project strategy was that some of the quiet technologies the team developed could be incorporated nearer term.

For the concept aircraft the community noise levels were estimated not to exceed 63 dBA for typical missions, comparable to the background noise in urban daytime environments. As described in [7] a substantial reduction (75 dB in cumulative Effective Perceived Noise (EPN) for sideline, take-off, and approach) was estimated relative to the Chapter 3 International Civil Aviation Organization (ICAO) noise standard. A description of the noise reduction technologies and enabling concepts is given in the next section. Predicted noise levels of the SAX-40, computed using standard Federal Aviation Administration (FAA) procedures, are compared to the existing fleet in Fig. 3.

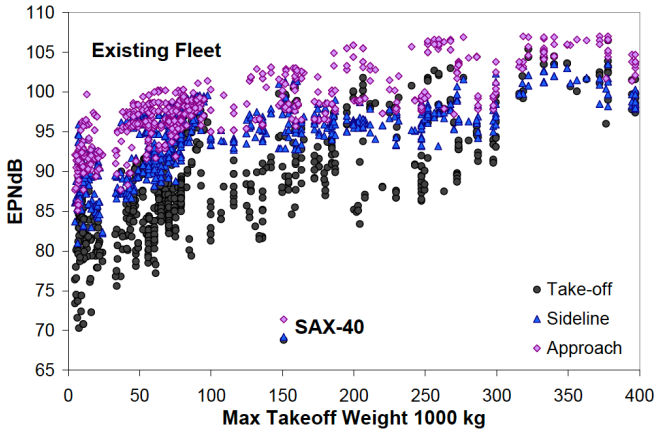

Fig. 3 Predicted SAX-40 noise levels relative to existing fleet [7].

The estimated fuel burn is shown in Fig. 4, in terms of energy usage per airline-seat-mile [7]. There is a major fuel saving predicted relative to current civil aircraft: 124 passenger-miles per (US) gallon which is 28% better than a Boeing 777 with a cabin configuration that delivers maximum passenger miles per gallon. For further comparison, a Toyota Prius hybrid automobile with two occupants would achieve 120 pax miles per gallon [8]. It is expected that further fuel efficiency, even with respect to this major saving, could be achieved in an aircraft design specifically targeted to minimize fuel consumption and emissions.

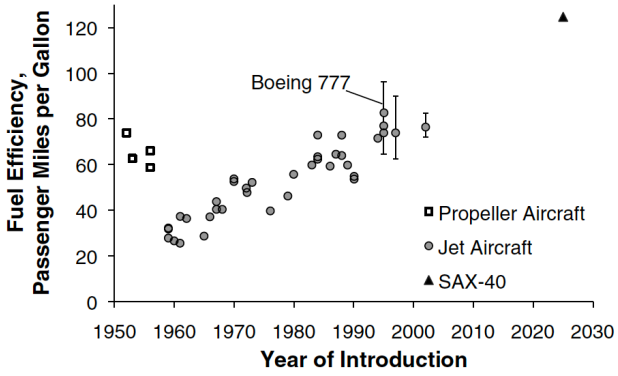

Fig. 4 Estimated fuel efficiency in terms of passenger miles per gallon [7].

3 Enabling Technologies for Noise Reduction

Low noise is not achieved by a single design feature but results from many disciplines integrated into the design and operation of a noise-minimizing aircraft system. These have been portrayed earlier in Figure 2, which is aimed at making the point that a number of different aspects of the aircraft must be altered to achieve the type of noise reduction sought [3,9]. Many of these design features are also beneficial in terms of reduced fuel burn and emissions.

The rationale for use of these features of the aircraft and the propulsion system can be summarized as follows:

- *Low noise approach operations*: On approach the airframe generates half the noise and the noise sources strongly scale with the flight velocity. Substantial noise reductions can thus be achieved by using a low speed approach and a displaced runway threshold on landing to increase the distance to the listeners on the ground [10].

- *Efficient airframe centerbody design*: The leading edge region of the centerbody is aerodynamically shaped to balance aerodynamic moments for pitch trim and to provide static stability without a tail [11]. At cruise conditions the all-lifting airframe is calculated to achieve an elliptical span load distribution, improving the Mach number times lift/drag ratio parameter (ML/D) by 15% compared to current blended-wing body type aircraft designs [7]. The enhanced low speed airframe performance allows to reduce the stall speed by 25% compared to current aircraft of similar size.

- *Airfoil trailing edge treatment*: Trailing edge brushes have been found to reduce the scattering noise from turbulence near the trailing edges [12]. The estimated trailing edge component noise reduction is 4 dBA.

- *Faired undercarriage*: The undercarriage noise sources can be mitigated by partially enclosing wheels and axles [13,14]. Estimated component noise reduction from use of fairings is roughly 6 dBA.

- *Deployable, drooped leading edge*: A deployable drooped leading edge can provide the required lift during low speed operations without the use of slats, thus eliminating slat noise. The drooped leading edge is stowed at cruise. Deployment power levels are comparable to a conventional slat. (This configuration is used on the Airbus A380.)

- *Quiet drag (needed on approach)*: Large wing area and high angle of attack provide the lift at low speed without using deployable flaps, eliminating a major source of airframe noise on take-off and landing. A combination of elevons and thrust vectoring can increase the induced drag to the required level, while trimming the aircraft. In addition, perforated drag plates could be deployed on approach, where the large scale flow structures responsible for the low frequency bluff body spoiler noise can be changed to small length scales driving turbulent mixing and surface interaction noise at frequencies not perceived annoying by the human ear [15]. Drag could also be achieved quietly by swirling the engine exhaust flow so as to create pressure drag. A full-scale turbofan demonstration of a deployable engine air brake (EAB) for drag management applications was recently reported stepping up the technology readiness level to that of a functional prototype (TRL 6) [16].

- *Embedded, aircraft boundary layer ingesting, distributed propulsion system*: Ingestion of fuselage boundary layer air into the engine allows a potential reduced fuel burn [17]. There is a trade between this gain and the losses due to the increased duct length needed for noise attenuation [18]. Embedding the engines within the airframe implies a high degree of airframe and engine integration. Engine airflow is now affected by the airframe and, similarly, the presence of the engines alters the flow around the aircraft. There are several major challenges, associated with the non-uniform flow into the engine (distortion), which must be addressed for a practical aircraft configuration [19]. The effects of boundary-layer ingestion on transonic fan rotor noise in a serpentine inlet is discussed in detail in Section 7.

- *Variable area exhaust nozzle to permit ultra-high bypass ratio, low fan pressure ratio, engines*: To reduce the engine noise at take-off the engine exhaust velocity must be decreased [20]. To ensure fan operability at the low power needed for low exhaust velocity the exhaust nozzle is designed to have variable area, with take-off bypass ratio of 18, and cruise bypass ratio of 12. The low engine rotational speed during approach enabled by the the variable nozzle reduces the rearward fan noise and the airframe drag requirements. The fan design, however, must now accommodate the broad range of flows associated with operation of low pressure ratio fans at different flight conditions. A change in fan design methodology was required to enable the fan to deal with the different conditions imposed by the variable area nozzle.

- *Airframe shielding of engine noise*: Placing the engines above the airframe prevents engine noise from reaching the observer. Engine forward radiated noise is virtually eradicated on the ground [21, 22].

- *Optimized take-off thrust management*: Thrust, climb angle, and nozzle area would be continuously varied during take-off to maintain a set noise level outside the airport boundary. This would allow the specified noise level to be met at all times during departure [23].

- *Optimized extensive liners*: The embedded propulsion system allows smaller engine diameter and thus increased non-dimensional (length/diameter) duct length. The longer inlet and exit ducts provide scope to further reduce engine noise by allowing additional acoustic liners, compared to conventional nacelles, to absorb the engine noise [18]. In the design configuration, use of an optimized multi-segment liner design results in an estimated 20 dBA reduction of engine noise.

A selection of two of the above ideas, namely placing engines above the airframe for noise shielding and boundary-layer ingestion through serpentine inlet ducts, will be discussed in some detail to illustrate the level of fidelity required in assessing the technologies and related challenges.

4 Beyond Silent Aircraft - NASA's Environmentally Responsible Aviation Program

Governed by concerns of aviation's impact on the environment and the rapid rise of fuel prices, NASA laid out a strategic roadmap for future aircraft concepts with stretch goals in fuel burn, emissions, and noise reductions for aircraft with potential entry into service dates of 2025 and 2035. As a consequence large scale, multi-team research projects, dubbed the N+2 and the N+3 (for second and third aircraft generations after next), were launched. Building on the momentum of NASA's early pathfinding study [2] a number of projects funded under NASA's Environmentally Responsible Aviation (ERA) project were launched. One of these projects, a collaboration between Boeing, MIT and the University of Califorina Irvine (UCI), built on the SAX-40 concept to conceive two N+2 vehicles. One of the outcomes was the definition of the N2A and N2B aircraft. The lower risk version, N2A, with two podded high-bypass turbofan propulsors mounted on top of the lifting hybrid-wing body airframe and between two vertical stabilizers is shown in Fig. 5. The higher risk version, N2B, much resembled the SAX-40 with an embedded

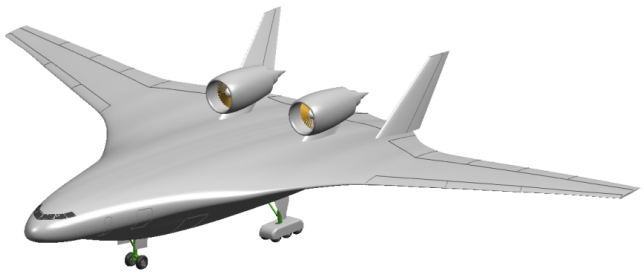

Fig. 5 NASA N+2 N2A aircraft with pod-mounted high bypass ratio propulsors.

distributed propulsion system. Both concepts were estimated to meet the fuel reduction goals and a 5.8% model of the full scale N2A vehicle with an extended trailing edge (EXTE) and engine simulators was assessed in the NASA Langley 14 by 22 foot wind tunnel as shown in Fig. 6. Details of the extensive aeroacoustic test setup can be found in [24]. Acoustic measurements were carried out for different aircraft flight conditions with the main focus on turbomachinery and jet noise shielding [25] and [26]. The turbomachinery broadband noise shielding results with the extended trailing edge indicated a 13 dB shielding benefit at peak frequency with at at least 10 dB benefit over a broad range of observer angles. It was also shown that the vertical tails provided shielding benefits as measured from the sideline while the noise below the aircraft was slightly increased. Both axisymmetric and chevron type nozzle sets were investigated and the unshielded chevron nozzle demonstrated 1 to 2 dB of source noise reduction. A shielding benefit of 6.5 dB of the axisymmetric nozzles was achieved at high frequency. The combined benefit of trailing edge shielding and low noise chevrons was measured to be up to 10 dB, exceeding

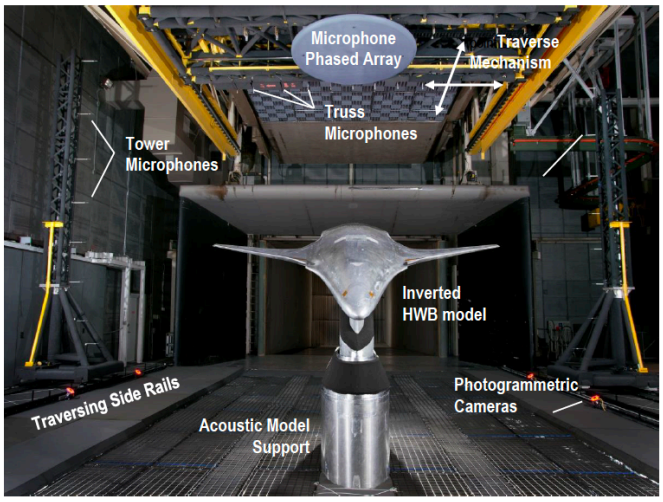

Fig. 6 Inverted N2A-EXTE model in NASA Langley 14 by 22 foot wind tunnel, figure adopted from [24].

the additive effects due to an effective upstream migration of the peak jet noise source location. In summary, a comprehensive overview of the NASA N+2 hybrid wing body aircraft concept, technologies, and system noise prediction development is given in [27] together with a portfolio of thirteen N+2 aircraft concepts.

Considering a potential entry into service date of 2035, MIT's D8 aircraft, also dubbed the "double-bubble" due to its non-round fuselage, was conceived under NASA's N+3 project in collaboration with Aurora Flight Sciences and Pratt & Whitney [28]. The D8 aircraft was designed for 180 passengers and a range of 3000 nm. Characteristic of the aircraft is the lifting fuselage, joined from two cylinders, and a pi tail. The two ultra-high bypass ratio engines are flush-mounted between the vertical stabilizers and ingest the fuselage boundary layer. Engine noise is shielded from the fuselage and the vertical tails and multi-segment extended liners. The first concept aircraft design assumed current engine technology and existing composite manufacturing techniques. Calculations estimate the D8 to be capable of saving 49% of fuel when compared with a Boeing 737-800. A second version, using advanced materials and manufacturing technology, with a potential entry into service date by 2035 was also designed suggesting 71% reduction in fuel burn. The benefit of the closely integrated propulsion system was experimentally demonstrated in back-to-back proof-of-concept tests of non-boundary layer ingesting and boundary layer ingesting versions of the D8 using 1:11-scale powered models in the NASA Langley 14- by 22-foot subsonic tunnel. The scale model of the D8 is depicted in Fig. 7. The aerodynamic benefit of boundary layer ingestion was measured to be 8.6% at the simulated cruise condition [29].

Part speed fan operation during takeoff, fan noise shielding from the fuselage and the vertical tails, and multi-segment, extended exhaust liners contribute to reduced propulsion system noise. The absence of leading edge high lift devices, a reduced approach velocity and steeper glide path, a faired undercarriage and the use of advanced materials and manufacturing processes, which reduce aircraft weight and therefore engine propulsive power at takeoff, enable substantial airframe noise reductions. Taking these design features in to account, a first assessment of the D8 aircraft concept suggested a community noise reduction of 60 EPNdB relative to FAR36 Stage 4 [30]. A more recent analysis by [31] indicates that, considering mid-term technology levels, the noise reduction potential is more likely near 33 EPNdB relative to Stage 4.

Fig. 7 NASA N+3 "Double Bubble" D8 aircraft model in NASA Langley 14 by 22 foot wind tunnel for performance assessment due to boundary layer ingestion, figure adopted from [29].

5 Challenges in Acoustic Assessment of Advanced Aircraft Configurations with Integrated Propulsion Systems

All of the advanced aircraft configurations and concepts introduced above have the propulsion system much more closely integrated with the airframe. This poses new challenges in the assessment of the noise sources and their acoustic signatures. For example: (i) the three-dimensional flow and non-axisymmetric geometries (flow distortion, component coupling etc.) inherently necessitate higher fidelity approaches, (ii) the length and time scale disparity between aerodynamics and acoustics require different numerical treatment, and (iii) the design studies demand fast turn-around times at adequate levels of fidelity. To facilitate an effective design space exploration compromises have to be made and modeling approaches compatible with design turn around time and system studies must be employed.

Low noise is not achieved by a single design feature or noise reduction technology but results from the integration of many concepts and ideas as listed earlier. The limited scope of this chapter only allow for a selected subset of technological challenges and related problems to be discussed at some length. Therefore only two technical problems and their assessments are outlined in more detail next. These were chosen because of their relevance and importance in advanced configurations and future aircraft concepts. Although different in nature both problems call for new approaches and careful treatment of the unsteady internal flows to enhance the ability to tackle the complex acoustic problems. The first problem is focused on quantifying the shielding of turbomachinery noise in unconventional aircraft configurations and the best placement and installation of the propulsion system relative to the airframe. Borrowing ideas from geometrical optics a diffraction integral method for fast assessment is briefly outlined. The second problem pertains to fan noise in serpentine inlets as seen for example in the boundary layer ingesting propulsion system of the SAX-40 aircraft as shown in Fig. 2. Due to the inlet flow distortion and related non-uniform flow the aerodynamics and acoustics are coupled and require simultaneous computation of the source noise generation, interaction of the fan and duct flow, and sound propagation. A new body-force based method is introduced to compute the fan shock noise in a fully coupled three-dimensional aero-acoustic calculation.

6 A Fast and Improved-Fidelity Method for Turbomachinery Noise Shielding

The N2A planform depicted in Fig. 5 potentially offers a turbomachinery noise shielding opportunity and an important question is that of the shielding benefit of a hybrid-wing-body type airframe. Furthermore, with the above-fuselage mounted propulsors, it is useful to assess the best engine placement and the impact of the vertical tails on shielding. Given the parametric nature of the study the shielding method must be compatible with design space exploration and yield a fast turnaround time. One option is the well known barrier shielding method which is a standard module in NASA's ANOPP aircraft noise assessment program [32]. The Beranek-Maekawa based barrier shielding correlation uses rectangular screens and therefore is fast but limited in geometry and fidelity as illustrated in Fig. 8 on the left for the N2A aircraft with a single noise source placed on the centerline [33,34]. A high-fidelity alternative would be to use for example NASA's fast scattering code which solves a three-dimensional boundary value problem to the Helmholtz equation [35], shown for the same airframe in Fig. 8 on the right. Inherently, the method is computationally costly and limited to low frequencies and therefore somewhat incompatible with turbomachinery noise.

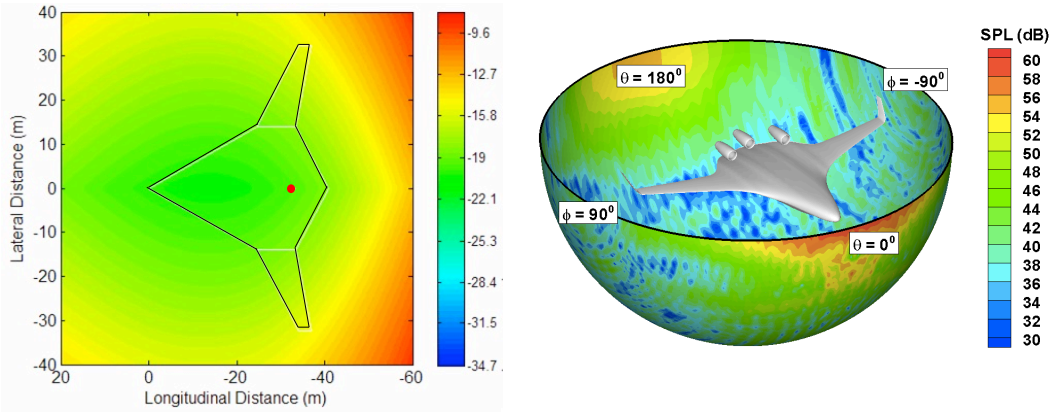

Fig. 8 Barrier shielding assessment (left) and fast scattering calculation [35] of a hybrid-wing-body aircraft (right).

6.1 The Diffraction Integral Method

To address these challenges a new shielding prediction framework based on the Kirchhoff diffraction integral approach was proposed. The fast method borrows ideas from the Modified Theory of Physical Optics (MTPO) and is capable of dealing with monopoles, dipoles, and directional point sources. Further, the potential describing the diffraction integral is formulated in terms of a Fresnel integral, which can be solved analytically to avoid costly numerical integration. Bulk flight effects are included and the method is validated against known, canonical test cases such as the shielding of a disk and a sphere. A short description of this method and the shielding assessment procedure are given below together with a parametric turbomachinery shielding study

of the N2A airframe. For more details and the theoretical development the reader is referred to [36] and [37].

To estimate the noise attenuation the sound field scattered by the shielding object is computed via the diffraction integral method using a boundary diffracted wave formulation. Considering the geometry in Fig. 9 and assuming that the incident field is undisturbed on the aperture (high frequency approximation), that the aperture has sharp edges, and that the screen is optically

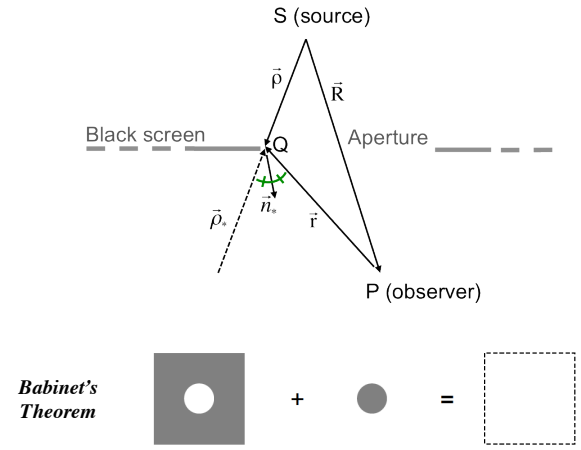

Fig. 9 Aperture in an infinite rigid screen (top) and Babinet's theorem (bottom): the diffraction around a shielding geometry can be calculated from the diffraction through an aperture of complementary shape.

black, the Modified Theory of Physical Optics (MTPO) yields the scattered field through aperture A:

$$p_s(P) = \frac{1}{4\pi} \iint_A [p_i(Q)\vec{n}_* \cdot \vec{\nabla}\frac{e^{ikr}}{r} - \frac{e^{ikr}}{r}\vec{n}_* \cdot \vec{\nabla}p_i(Q)]dS, \tag{1}$$

where p_s and p_i are the scattered and incident fields respectively, $\vec{n}_*$ is the modified normal splitting the angle between the diffracted ray and image of the incident ray, and r is the distance between the point of integration and the observer P. The field scattered by the object complementary to the aperture is obtained by applying Babinet's principle as illustrated in Fig. 9 on the bottom. This principle provides a way to interchange aperture and screen and states that the sum of the diffracted fields of complementary screens is equal to the free field. Thus, the diffraction around a shielding geometry can be calculated from the diffraction through an aperture of complementary shape based on the difference

$$p_s^{object}(P) = p_i(P) - p_s^{aperture}(P). \tag{2}$$

Instead of evaluating the computationally expensive diffraction surface integral in Eq. 1, the Diffraction Integral Method is based on a line integral formulation of the boundary-diffracted waves. The boundary-diffracted wave theory states that the scattered field can be interpreted as the combined contribution of the undisturbed geometrical optics field and the boundary-diffracted wave field

$$p_s(P) = p_{GO}(P) + p_d(P). \tag{3}$$

where $p_{GO}(P) = p_i(P)\chi(P)$ and $\chi(P)$ is the unit step function. The unit step function assumes value one when the ray between the source and the observer passes through the aperture, and value zero otherwise. Using vector analysis an expression for the boundary-diffracted wave can be derived based on the MTPO surface integral. The resulting diffraction potential allows for source directivity and becomes

$$p_d(P) = \frac{1}{4\pi}\oint_C p_i(Q)\frac{e^{ikr}}{r}\frac{(\vec{\rho}\times\vec{r})\cdot d\vec{s}}{(\vec{n}_*\cdot\vec{n})(\rho r+\vec{\rho}\cdot\vec{r})} \tag{4}$$

where p_d is the boundary diffracted wave field and C is the integration contour along the source line-of-sight.

The MTPO based diffraction potential was derived assuming sharp edges and the curvature of the fuselage and wing leading edges is likely to impact the shielding level at low frequencies. A creeping wave extension to the method was introduced to capture diffraction at curved edges with the aim to maintain simplicity and computational efficiency of the present framework. To do so the local object geometry with a round edge was approximated with a least square fitted cylinder. The diffracted field can then be described using an alternative line integral potential corresponding to round-edge diffraction, derived from the Geometric Theory of Diffraction (GTD) [38]:

$$p_d^{CW}(P) = \sqrt{\frac{2k}{\pi}}e^{-i\frac{\pi}{4}}\oint_C \sum_m D_m^2(k,a)e^{-ta_m+ikt}p_i(Q)\frac{e^{ikr}}{r}ds, \tag{5}$$

where D_m^2 and α_m are the m-th order diffraction and decay coefficients, a is the local radius of curvature and t the length of the ray path along the cylinder.

The Diffraction Integral Method is suitable for incorporation in aircraft noise prediction programs and is executed in two steps via an "online part" and an "offline part". The online part solves the contour integral during aircraft noise calculations so that the aircraft noise prediction program can apply the calculated noise attenuation to the estimated turbomachinery noise. This setup allows the offline part to be executed only once for a particular airframe shielding geometry while the online part is carried out for every observer location and source frequency. The offline part specifies the source description, flight conditions and shielding object geometry, and computes the shielding contour on the object. The shielding contour is defined as the outline separating the illuminated and shadow regions of the object as seen from the source, illustrated in Fig. 10 on the left. A robust integration contour search algorithm was developed [22], applicable to a broad range of airframe geometries as demonstrated in Fig. 10 on the right. The central idea of the algorithm is to represent the line of sight of the noise source by projecting the coordinates of the object along rays emanating from the noise source onto a sphere. This sphere is centered around the source and the projection reduces the problem to two dimensions. The outermost outline extracted from the projection, when transformed back to the original three-dimensional coordinates, is the outline on the surface of the object as viewed by the source as depicted in Fig. 11.

6.2 Turbomachinery Noise Source Description

The effect of mean flow on the sound field produced by acoustic sources and sound-scattering bodies can be important. The idea is to modify the time and space variables to account for the translation of the source and the shielding body. To capture the bulk flow effect on shielding, a non-linear transformation similar to the Prandtl-Glauert approach was used [37]. Due to the non-linearity in flight Mach number, this transformation requires the scattering computation

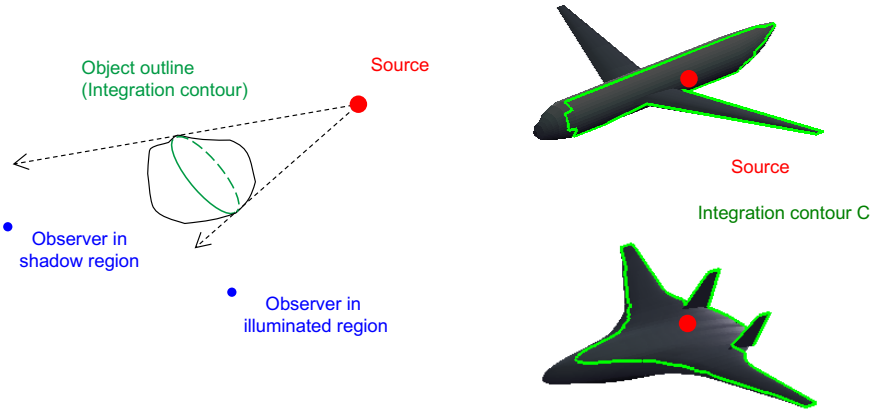

Fig. 10 Robust integration contour search algorithm.

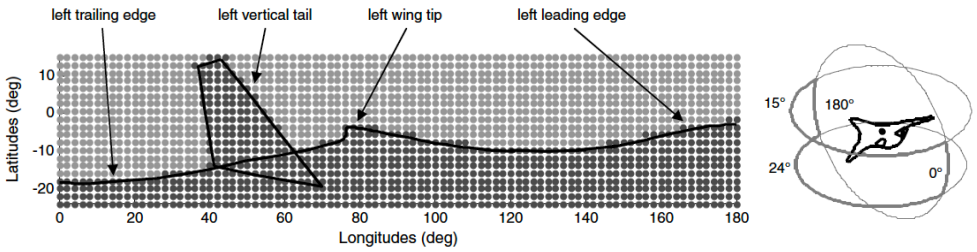

Fig. 11 Unwrapped projection of illuminated (grey) and shadow (black) regions on to a hemi-sphere centered around the source - the shadow boundary is traced back to the object to define the integration contour (black line, which is the green line in Fig. 10). Note: low resolution grid density is just for illustration purposes.

to be carried out at the Doppler shifted frequencies. The transformation is valid for small flow perturbations and for harmonic waves.

Most current shielding methods are based on monopole sources. While monopole sources are computationally efficient and simple to implement, turbomachinery noise is directional by nature and requires a higher fidelity description. Directivity functions are commonly used in empirical noise source formulations such as for example the Heidmann fan noise module HDNFAN in ANOPP [39]. However, it is important to note that such directional point source formulations only satisfy the Helmholtz equation in the far field and can yield significant errors in the near field. To avoid these errors and to ensure that the Helmholtz equation is satisfied everywhere, the directional point source is written in terms of spheroidal functions using a least squares fit. This is what is called the Helmholtz Equation Least Squares (HELS) approximation [40]. Fig. 12 compares the far field polar directivity patterns of the ANOPP fan module with the corresponding HELS field reconstructions at 50 Hz and 10kHz respectively. The spheroidal functions allow the HELS representation to estimate the near field which governs the diffraction around the integration contour and therefore noise shielding. For the directional point source based on the ANOPP fan module the shielding errors can be as high as 18 dB in the near field (not shown

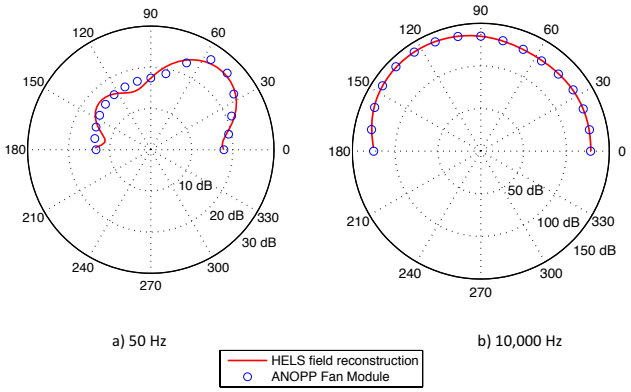

Fig. 12 Comparison of far field polar directivity patterns: ANOPP HDNFAN fan module and corresponding HELS field reconstruction for a) 50 Hz and b) 10kHz..

here), illustrating the importance of the HELS based near field reconstruction. More detail of the HELS representation and near and far field assessment can be found in [37].

6.3 Method Validation and Hybrid-Wing Body Aircraft Shielding Assessment

The diffraction integral method was first validated against NASA's Fast Scattering Code (FSC) [41] on two canonical shielding geometries: a sphere and a circular disk. A monopole source was implemented in this validation, consistent with the FSC approach. The comparison was carried out for Helmholtz numbers ranging from $ka = 1$ to $ka = 400$. Fig. 13 summarizes the assessment for $ka = 92$. The results for the disk case on the right demonstrate that the diffraction integral method is in good agreement with the FSC results. The maximum error of about 2 dB occurs at ka=194 (not shown here). The sphere shielding cases exhibit larger discrepancies between the methods and can reach up to 7 dB. This suggests that at high frequencies ($ka > 92$), as expected per the assumptions, the diffraction integral method yields relatively small errors for flat geometries with sharp edges. Larger discrepancies occur in the case of round shielding objects which are due to creeping-ray diffraction. Using the creeping wave diffraction potential from Eq. 5 this error can be reduced as illustrated in Fig. 14 where the Diffraction Integral Method is compared with an analytical shielding solution of the sphere for Helmholtz numbers $ka = 92$ and $ka = 194$. The results are encouraging and future work is focused on making the formulation, especially in the transition region, robust for more realistic geometries such as airframe leading edges.

The Diffraction Integral Method was next applied to the NASA N2A Hybrid-Wing Body aircraft configuration to demonstrate its applicability to advanced aircraft configurations and to investigate the impact of source directivity on noise attenuation. The N2A aircraft geometry, the source location (red dot) and the corresponding shielding outline (green) in Fig. 10 were used in the assessment. The observer plane was located 30 m below the aircraft and the far field noise was assessed at the standard 24 1/3-octave band center frequencies according to FAR36 regulations.

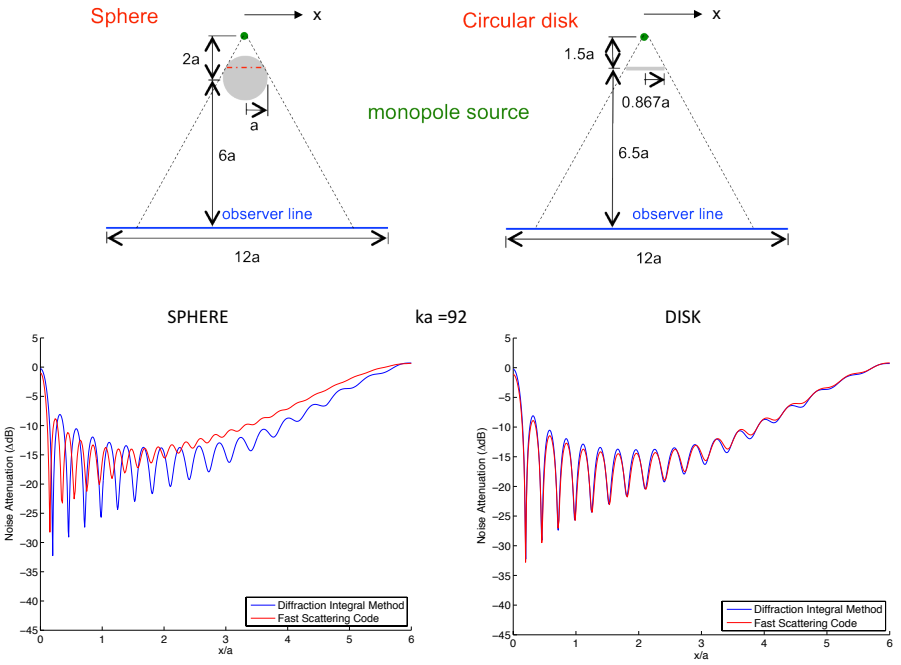

Fig. 13 Shielding comparison between DIM and FSC methods at $ka = 92$: sphere (left), disk (right).

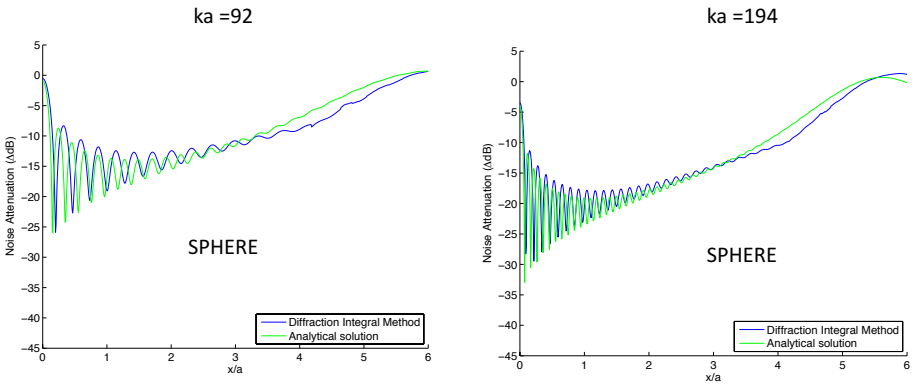

Fig. 14 Shielding results for sphere at $ka = 92$ and $ka = 194$: DIM with creeping wave diffraction vs. analytical solution.

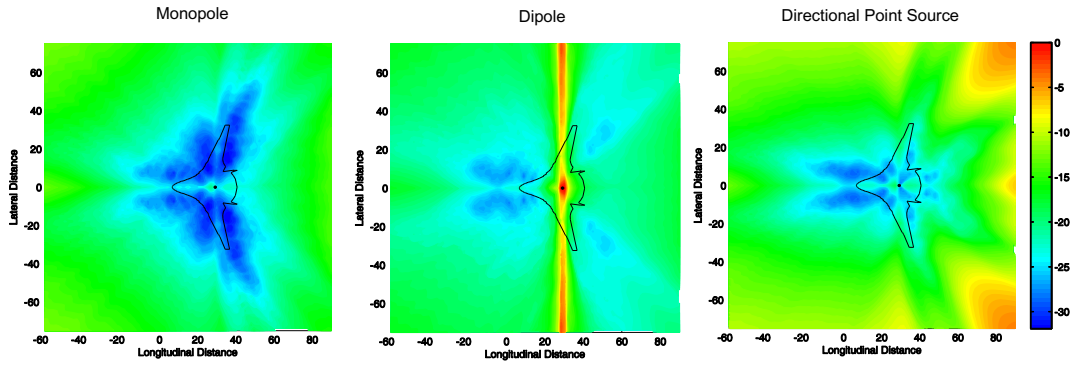

Fig. 15 Shielding patterns and insertion loss (in dB) for a monopole, a dipole, and a directional point source description using the HELS reconstruction.

Computations were carried out for a monopole, a dipole aligned with the flow direction, and a directional point source using the HELS reconstruction. The Heidmann fan noise model was used in the directional point source description with directivity according to Fig. 12. As shown in Fig. 15 both computations predict high levels of shielding of up to 30 dB in the forward and aft directions. In the lateral direction the monopole based shielding calculation overestimates the insertion loss by up to 12 dB. This is partially due to the higher sound pressure level in this direction in the case of the monopole. An increase in insertion loss is observed in the case of the dipole in the lateral directions, where the incident field approaches zero. This is suggested to be due to the redistribution of acoustic energy by the outline which acts like a line source.

Four HWB aircraft configurations with different engine placements, vertical tails, and winglets were then assessed to determine the best propulsion system integration from a perspective of turbomachinery noise shielding. In the baseline configuration the noise source was located on the centerline of the aircraft, $0.71c_0$ aft of the nose and $0.1c_0$ above the chord, where c_0 is the wing root chord length. The other three configurations assessed the effects of moving the noise source along the centerline, adding winglets, and adding vertical tails to the baseline HWB aircraft as depicted in Fig. 16. The noise attenuation computed by the diffraction integral method along the centerline (at $y = 0$) and sideline (at $y = 45$ m) are captured in Fig. 17 and allow for a direct comparison between the four HWB aircraft configurations. The results suggest that the baseline HWB aircraft a) can provide up to 22 dB reduction in OASPL, about 7 dB more than the conventional tube-wing airframe shown in Fig. 10.

In configuration b), the noise source was moved aft by one engine diameter, or about $0.06c_0$. The overall amount of noise attenuation is reduced because the noise source occupies a less central position on the airframe. In general, noise attenuation is reduced as the noise source is moved closer to the diffraction edge consistent with the findings in [25]. The effect of adding winglets to the HWB aircraft, configuration c), does not alter the noise attenuation appreciably, because of the proximity of the noise source to the airframe: the noise attenuation in the area of interest, i.e., around the centerline and sideline, stems mostly from the centerbody and not the outer wings. Therefore, the winglets have negligible effect, except in the far lateral direction (not shown here). This suggests that vertical tails located closer to the centerbody can contribute to the geometric shadow region to increase shielding, as indicated in Fig. 17. This is consistent with

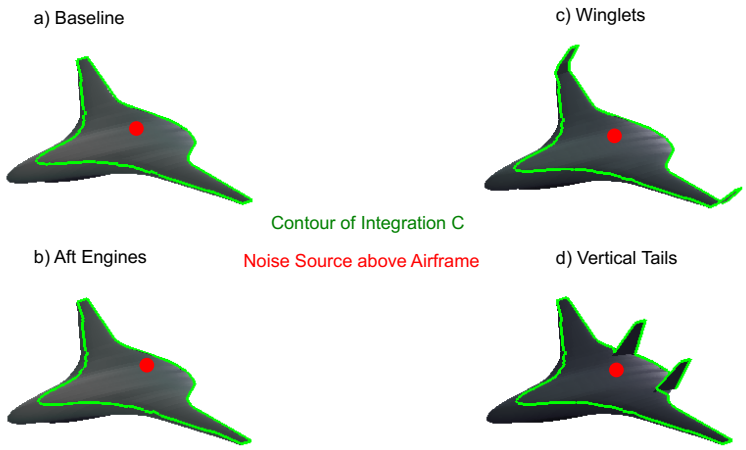

Fig. 16 HWB aircraft configurations for turbomachinery noise shielding assessment: a) baseline, b) with noise source moved aft, c) with winglets, and d) with vertical tails.

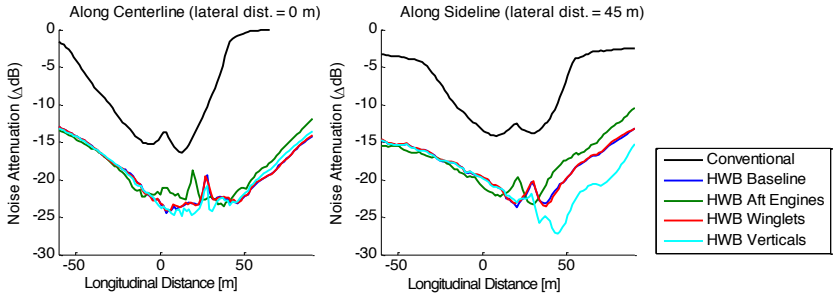

Fig. 17 Line plots of noise attenuation computed by the diffraction integral method for different HWB aircraft configurations along the centerline and along the sideline.

the experimental findings in [25] where the effects of engine location and vertical tail configuration on the shielding of the broadband component of turbomachinery noise for a HWB aircraft configuration were examined.

In summary, borrowing ideas from geometrical optics a diffraction integral method for fast, improved fidelity noise shielding assessment capability was introduced. A robust integration contour search algorithm, applicable to a wide range of geometries, was developed to determine the outline of the shielding contour separating the illuminated region from the shadow region. The evaluation of the diffraction line integral along this contour was cast in terms of a Fresnel integral, which can be solved analytically. This facilitates the program to run on the order of seconds on a laptop computer and enables rapid assessment of unconventional airframe and propulsor configurations at much improved fidelity relative to the standard barrier shielding methods.

7 Effects of Boundary-Layer Ingestion on Transonic Fan Rotor Noise

Embedded propulsion systems facilitate boundary layer ingestion which has proven substantial fuel burn reductions but the interaction of the boundary layer with the fan poses both aerodynamic and acoustic challenges. Distortion tolerant fan designs are being pursued to mitigate the fan isentropic efficiency penalties and operability challenges. The ingestion of the incoming boundary layer through a serpentine duct, as shown in Fig. 18, and subsequent interaction with the fan rotor complicates the aero-acoustic modeling and noise assessment. Fan rotors with supersonic relative flow at the blade tips generate rotor shock noise. This tonal noise is caused by small blade-to-blade variations inherent to the manufacturing of fan blades. The result is a rotor-locked shock structure at shaft frequency propagating upstream through the inlet and radiating noise to the far field. The so-called "buzz-saw" or multiple pure tone (MPT) noise is especially prominent during take-off and strongest at cut-back flight conditions. In nonuniform flow, the generated shocks have varying strengths and propagation directions which can have dramatic implications both on the source noise and the perceived far field community noise.

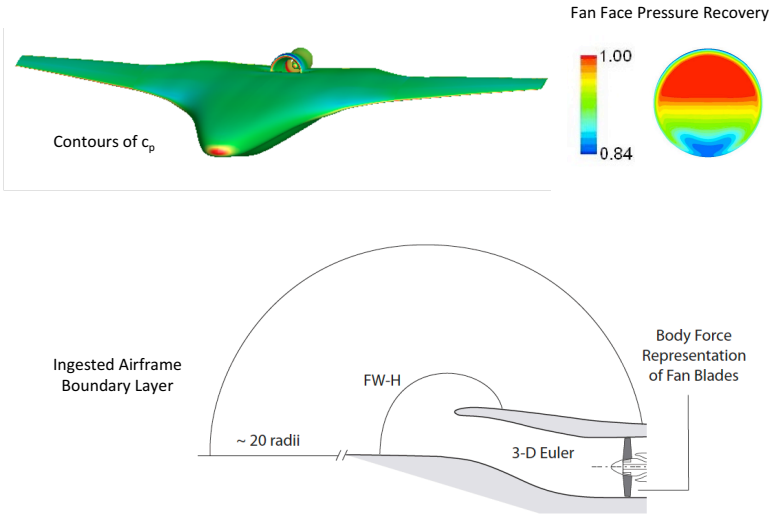

Fig. 18 Boundary layer ingesting embedded propulsion system: gap in length and time scales between aerodynamics and acoustics bridged via three-dimensional unsteady Euler calculation combined with body force based source noise generation.

The aerodynamics and acoustics of the problem are inherently coupled and the MPT noise consists of non-linear waves in the near field of the fan. An innovative approach was conceived to numerically simulate the transfer of inlet flow distortion through the fan stage due to BLI and the generation and propagation of the resulting MPT noise. A body force method was used to represent the fan blade row in a 3-D full-wheel unsteady Euler calculation as illustrated in Fig. 18 on the bottom. The computational domain includes both the inlet and fan rotor region and the external flow region for acoustic propagation. The body forces respond locally to the flow conditions such that the force field is non-uniform when subjected to a distorted inlet flow due to ingestion of the airframe boundary layer. This approach allows for computationally effective

MPT noise assessment of highly integrated propulsion systems and advanced inlet configurations using unsteady full-wheel calculations.

7.1 Body Force Based Multiple Pure Tone Source Noise Generation

The key idea is to represent the fan rotor with a rotating body force field that generates rotor shock noise; its time-mean component provides the quasi-steady pressure rise and flow turning of the rotor. A single-passage, steady 3D Reynolds-averaged Navier-Stokes (RANS) calculation of the fan rotor was first carried out to obtain the body-force-based description of the blade row performance. The body force field description thus obtained can respond locally to the flow conditions such that the effects of inlet distortion are captured. The body force field was then perturbed by a rotor-locked disturbance to create rotor shock noise. This perturbation, its shape derived from the 3D RANS calculation, is periodic over one blade pitch and generates the blade leading edge shock and expansion fan system. In addition, a rotating disturbance field

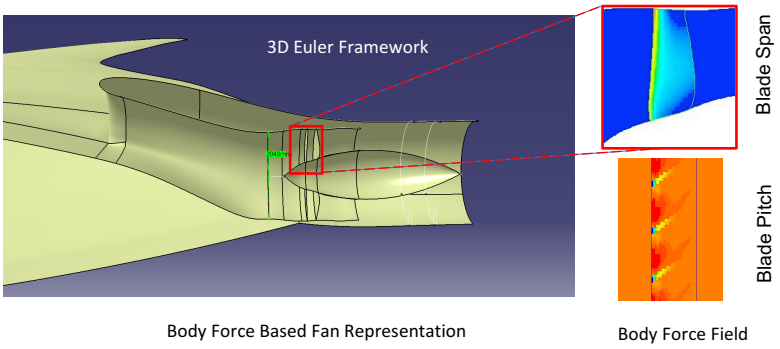

Fig. 19 Rotating body force field generates blade leading edge shock and expansion fan system.

with once-per-revolution periodicity is introduced to generate variations in this shock system and thus MPT noise. A cut-away of the serpentine inlet duct and body force field domain used in the calculations are shown in Fig. 19.The amplitude of the variations was obtained from a perturbed 2D cascade RANS calculation. To illustrate the idea, the full body force formulation is given here for the axial force component

$$f_x(r,x,\theta,t) = \overline{f_x}(M_{rel}(r,x,\theta),\alpha(r,x)) + \delta f_x(r,x,\theta-\Omega t). \tag{6}$$

The first term is the local time-mean force component which contributes to the quasi-steady pressure rise and flow turning and depends on the local relative Mach number, M_{rel}, and local blade camber angle, α. The second term is the perturbation to the body force,

$$\delta f_x(r,x,\theta-\Omega t) = \overline{f_x}(M_{rel},\alpha)\cdot(1+\epsilon)\cdot S(r,x,\theta-\Omega t), \tag{7}$$

where ϵ is the perturbation due to stagger angle changes from one blade passage to another, and S is the perturbation function that creates the shock-expansion fan system.

The body force formulation was implemented in a full-domain unsteady Euler calculation and the far-field noise was determined via the Ffowcs-Williams and Hawkings (FW-H) integral method using a permeable surface. A more detailed description and validation of this approach can be found in [44].

7.2 Validation of Body Force Based MPT Noise Prediction Method on a Conventional Inlet-Fan Configuration

To validate the approach the NASA/GE R4 rotor with 22 rotor blades was considered at the cutback operating condition (87.5% corrected design speed). The fan exit guide vanes were not included in this analysis although the methodology could be extended in the future to capture blade-row interaction noise. The fan exhaust was ducted out of the computational domain to prevent fan exhaust noise from contributing to the far field noise levels. Fig. 20 a) and b) demon-

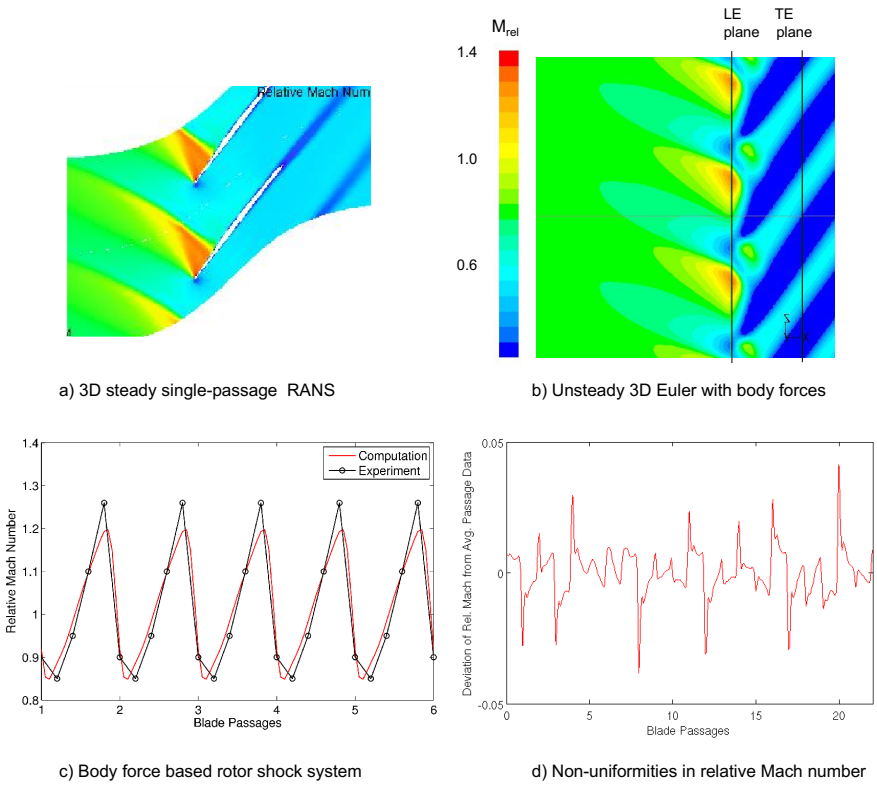

Fig. 20 NASA/GE R4 rotor flow field at 92% span: a) single-passage RANS calculation, b) rotating body force based shock structure, c) validation of body force calculation with measurement, and d) perturbed rotating body force based non-uniformities in relative Mach number which lead to MPT noise.

strate that the required rotor-locked field of expansion fans and shock waves can be generated by the body force model, including the blade-to-blade stagger angle perturbation. Experimental measurements of the rotor flow field [45] were used to assess the capability of the model to accurately generate the rotor-locked shock structure. Fig. 20 c) depicts the experimental and computed relative Mach number at 92% span, 1/4 chord upstream of the rotor leading edge. Both results represent average passage distributions with the effects of nonuniform blade stagger removed, since the exact blade stagger angle variations in the experimental rotor were unknown. The computed saw-tooth like pattern is in good agreement with the measurement with slightly shallower slopes in relative Mach across the expansion fan. The lower, rounded peaks are due to the spatial filtering of the governing equations in the body force method. The computed relative

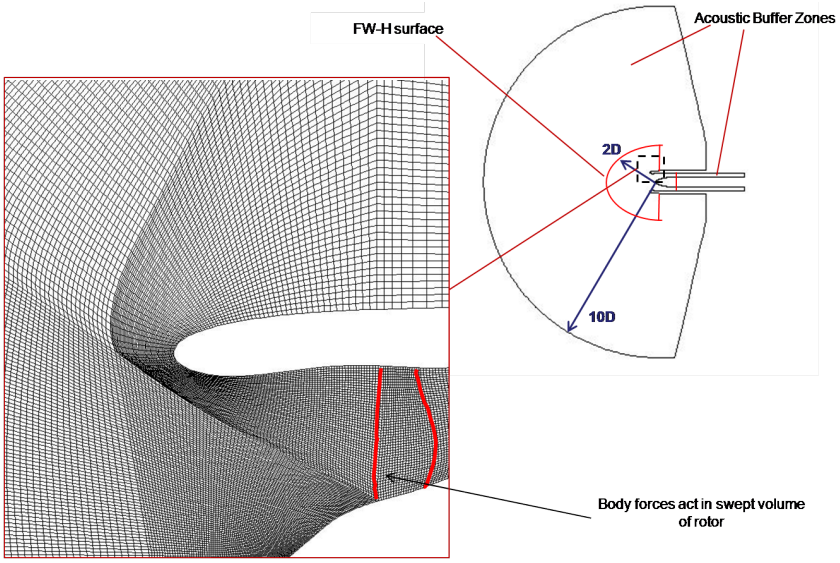

Fig. 21 Computation domain and setup for NASA/GE R4 far-field MPT noise validation assessment.

Mach number at the same location for the full wheel is given in Fig. 20 d), illustrating the non-uniformities which lead to MPT noise. Using this three-dimensional shock structure, acoustic computations were carried out for a total of 14 rotor revolutions to assess the in-duct mode propagation far-field noise signature; acoustic data was recorded only for the final 5 revolutions to ensure that all transients were settled.

To assess the capabilities of the body-force based MPT noise prediction methodology, a validation case was carried out using NASA Source Diagnostic Test (SDT) data for the model-scale GE R4 rotor in a rotor alone configuration as shown in Fig. 21. The computational domain consisted of the fan, upstream and downstream ducts, and upstream far-field region. To eliminate spurious reflections acoustic buffer zones were implemented. The computational grid was approximately 17 million cells and more detail can be found in [44]. The new methodology was assessed in its ability to predict the far-field MPT noise levels against NASA SDT data reported in [46]. Fig. 22 shows spectra at various receiver locations, specified by emission angle, for both the computation and the experimental data. The sound levels of the MPTs and in particular their level relative to the blade-passing tones are in agreement. The specific frequencies at which MPTs occur are not expected to be the same since the fan blade stagger angle distributions in the experiments were not identical to those in the computation.

7.3 Effects of Boundary-Layer Ingestion in Serpentine Inlets on MPT Noise

With the framework validated and assessed, the SAX-40 airframe with a single serpentine inlet and fan shown in Fig. 18 was implemented. The same NASA/GE R4 rotor was used and the computational grid and buffer zone domains followed the setup of the conventional inlet case.

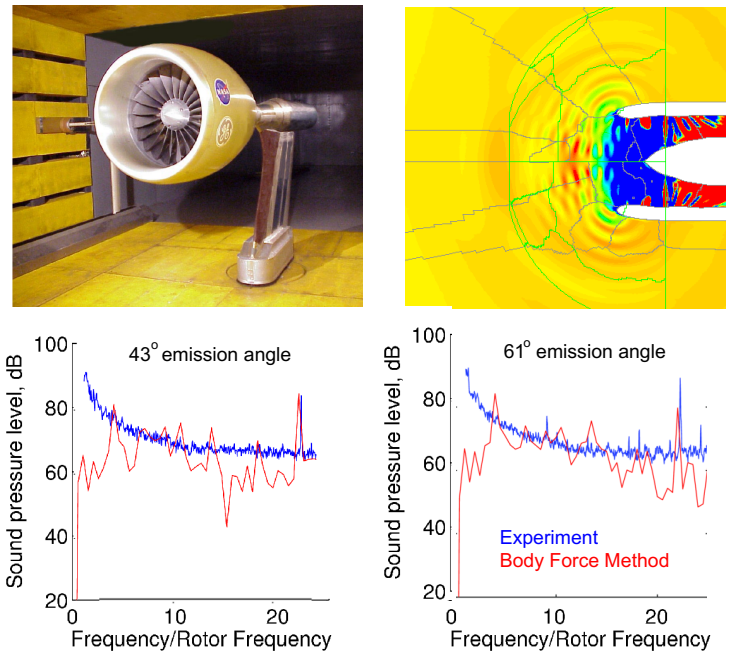

Fig. 22 NASA/GE R4 fan rotor acoustic test [46] (top left) and computed instantaneous acoustic pressure field (top right). Sound spectra at two different emission angles (bottom): computed ratio of multiple-pure-tones to blade-passing tone amplitude in good agreement with experiment.

The key difference though was the inclusion of the boundary layer flow of the airframe suction surface. More detail of the implementation can be found in [19] and [47].

At the low-speed condition with a free-stream Mach number of 0.1 there is approximately 20% BLI and the inlet pressure recovery is equal to 0.99. The Mach number at the aerodynamic interface plane (AIP) just upstream of the rotor is approximately 0.5, so that the flow accelerates into the inlet at the low-speed condition. Thus, at low flight speeds the ingested vorticity in the boundary layer is more important than the stagnation pressure deficit. While this vorticity is perpendicular to the flow direction well upstream of the inlet, as it interacts with the inlet lip it is tipped into and stretched along the streamwise direction as depicted in Fig. 23. The streamwise vorticity is enhanced by the stretching of the vortex lines as the flow accelerates into the inlet. The result is the creation of regions of high-speed flow centered around the vortex cores.

The blade shock strength is governed by the incoming relative Mach number and relative inlet flow angle, which can be perturbed by stagger angle changes and more dominantly inlet flow distortion. An unwrapped view of the instantaneous relative Mach number field at 92% span is depicted in Fig. 24 for both the conventional and the serpentine inlet computations, extending from the fan leading edge to the aerodynamic interface plane. In the bottom plots, small variations in shock strength and angle can be observed due to the blade-to-blade variations in stagger angle. This is the source of MPT noise in undistorted inlet flow. The maximum variation in peak relative Mach number due to the stagger angle variations is 0.04. With inlet distortion present in the top plot, regions with co- and counter-swirl result in relative Mach number variations of as much as 0.32, approximately eight times larger than the variation due to stagger angle alone. Furthermore, the region of co-swirl leads to subsonic relative Mach numbers

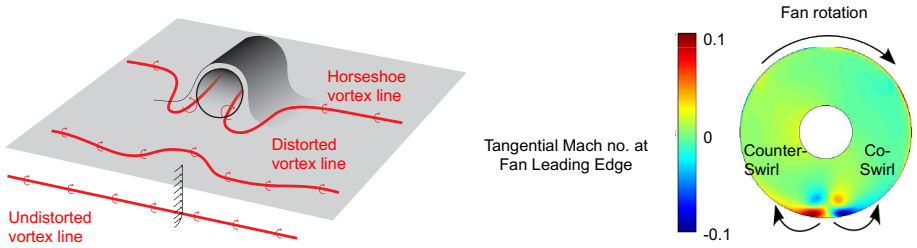

Fig. 23 Generation and ingestion of streamwise vorticity due to boundary-layer ingestion: the two legs of the ingested horseshoe vortex induce regions of co- and counter-swirl at the fan face.

(dark blue region), whereas counter-swirl increases the supersonic relative Mach number (yellow region) yielding stronger shocks. This is also manifested in the angle changes of the wave fronts or the corresponding perpendicular wave number vectors: wave fronts inclined further away from the axial direction correspond to increased wave propagation rates while those angled closer to axial propagate at reduced rates, becoming evanescent in the limit of a purely tangential wavenumber vector.

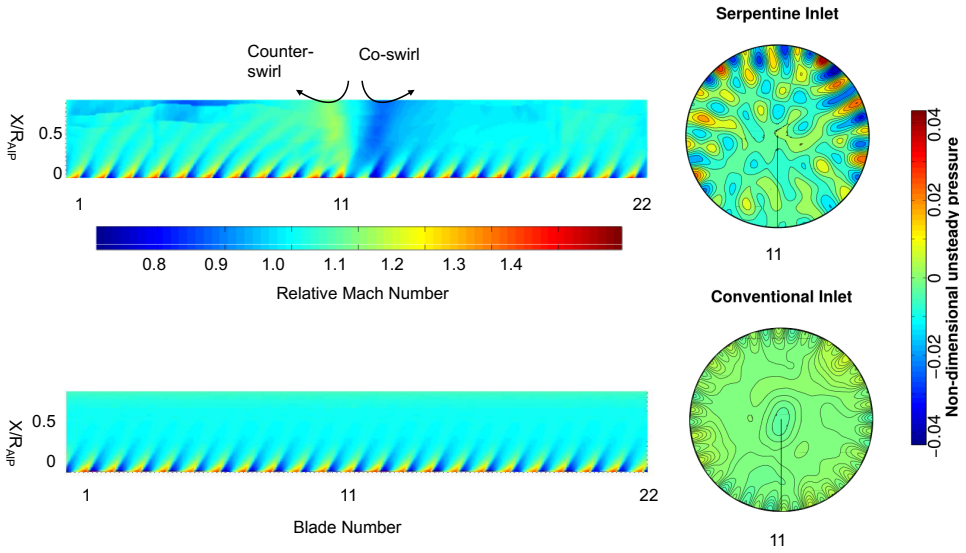

Fig. 24 Serpentine vs. conventional inlet: relative Mach number at 92% span from fan LE to AIP (left) and unsteady pressure at AIP over mean dynamic pressure at AIP (right). The counter-swirling vortex strengthens the shocks and increases the source noise.

The nonuniform inflow condition has a more pronounced effect on shock strength and variation than the stagger angle variations, increasing the amplitude of shaft-order components of the pressure field. The consequence is an increase in fan sound power level of 38 dB for the serpentine inlet compared to the conventional inlet case. In addition to the increased sound pressure level, a

qualitative change in the unsteady pressure field occurs during upstream propagation. Some of the acoustic modes have decayed at AIP. This is conjectured to be due to the presence of the subsonic relative flow region induced by the co-swirling streamwise vortex since the subsonic relative flow results in locally evanescent wave behavior as shown in Fig. 25. Furthermore, the blade-passing circumferential modes are cut-off while a mode with circumferential extent of roughly two blade pitches is dominant and significantly enhanced in sound pressure relative to that of the rotor leading edge. Note that the streamwise vorticity due to boundary layer ingestion is concentrated over about 2 blade pitches, or 1/11th of the circumference. This suggests coupling between the inlet distortion and the duct dynamics, where acoustic modes with spatial frequency equivalent to that of the distortion pattern are excited and scattered.

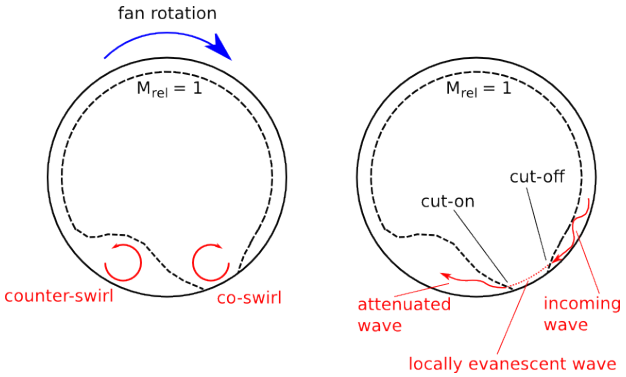

Fig. 25 Subsonic region attenuates wave propagation: cut-off and cut-on behavior due co-swirling vortex.

For the serpentine inlet, the duct extends further upstream from AIP, and Fig. 26 on the left depicts the unsteady pressure field at the throat near the inlet plane of the serpentine duct. High spatial harmonic modes have vanished, and the unsteady pressure field is dominated by long-wavelength, low-frequency waves, which remain cut-on. The decay from AIP to the inlet plane is approximately 15 times less than that from the fan face to AIP, although the streamwise distance is approximately four times longer. The decreased decay rate upstream may be linked to the increasing streamwise vorticity due to vortex stretching as the flow approaches the fan. The small areas of concentrated pressure visible on the lower surface in the figure are numerical effects due to imperfect geometry discretization.

The full-scale spectra for the conventional and serpentine inlets at 48 degree emission angle in Fig. 26 on the right reveal two striking results. Firstly, frequencies greater than 11 times the shaft frequency, including the blade passing frequency (BPF), are absent for the serpentine inlet case, suggesting that they are cut-off in the inlet. This is consistent with the sound pressure field observed at the inlet plane shown on the left. Secondly, the sound pressure level for frequencies less than 11 times shaft frequency are elevated due to the interaction of the inlet flow distortion with the fan rotor and the propagation of acoustic waves through nonuniform background flow. While the average linear OASPL is 7 dB higher for the serpentine inlet, due to the concentration of acoustic energy at low frequencies, A-weighting the spectra results, on average, in only 3 dBA higher OASPL for the serpentine inlet case. It is important to note though that the presence of the airframe acts as a reflecting surface and, therefore, the A-weighted sound power essentially

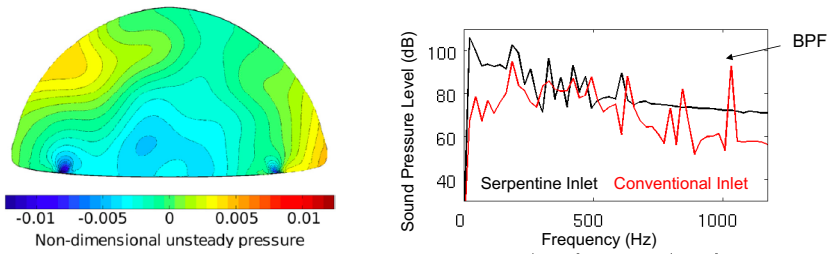

Fig. 26 Unsteady pressure at serpentine inlet face over mean dynamic pressure at AIP (left) and full-scale far field sound pressure level (right): far-field spectra amplified below 1/4 BPF and tones above 1/2 BPF attenuated (cut-off) relative to conventional inlet. Boundary layer ingestion in serpentine inlet increases average OASPL by 7 dB (3 dBA).

remains the same for the two cases. To reduce far-field noise, it may be possible to take advantage of the underlying mechanisms to redistribute the acoustic energy to low frequencies at which the human ear has reduced sensitivity. The results also emphasize that airframe shielding is critical for embedded propulsion system configurations as discussed earlier, especially if the source noise is dramatically increased such as through boundary layer ingestion.

8 Outlook: From Ultra-Low Fan Pressure Ratio Propulsors to An Electrified Future of Aviation

The advent of low fan pressure ratio (FPR) propulsors has somewhat redefined the aircraft noise challenge. Jet noise has become less of a concern while fan, core, and airframe noise have become more prominent. As the large engine bypass ratios increase the fan diameter, innovative nacelle concepts with short inlets are required to reduce their weight and drag. To take advantage of the propulsive efficiency benefits of the next generation ultra-low FPR propulsors, the current inlet length-to-diameter ratios of about 0.65 to 0.7 will have to be reduced to less than half their value [42]. This has an impact on inlet design, both aerodynamic and acoustic. The wetted inlet area available for acoustic liners will be dramatically reduced and the more non-uniform inlet flows will alter the acoustic propagation characteristics of the inlet duct. It is clear that novel modeling approaches, new liner concepts, and technologies to mitigate fan and core source noise will have to be employed to meet the design requirements. The electrification revolution has been spreading across the transportation domains from rail systems to electric and hybrid cars, personal transport, and more-electric ships and aircraft. In particular fully electric, turbo-electric, and hybrid electric propulsion systems are currently being investigated for commercial air transportation. While small vehicle demonstrations at the level of hundreds of kW are successfully progressing, it is unclear how the electrical machines and related components scale to levels of tens or hundreds of MW. Another question to be answered is the appropriate level of hybridization given that current and future battery energy densities range from 150 to 600Wh/kg [43] whereas kerosene has an energy density of about 12,000Wh/kg; at 50% gas turbine efficiency its effective energy density is 6,000Wh/kg. To reap the potential benefits of electrification and hybridization boundary layer ingestion, distributed propulsion and much more closely integrated airframe propulsion systems will be required. Independent of the type of prime mover, be that a battery powered electric motor, a hydrocarbon fueled turbo-electric system, or a hybrid architecture with a mix of hydrocarbon and battery based energy sources the challenges will be similar: while the future of electrification of aviation is uncertain, the physics of unsteady flow and the principles of

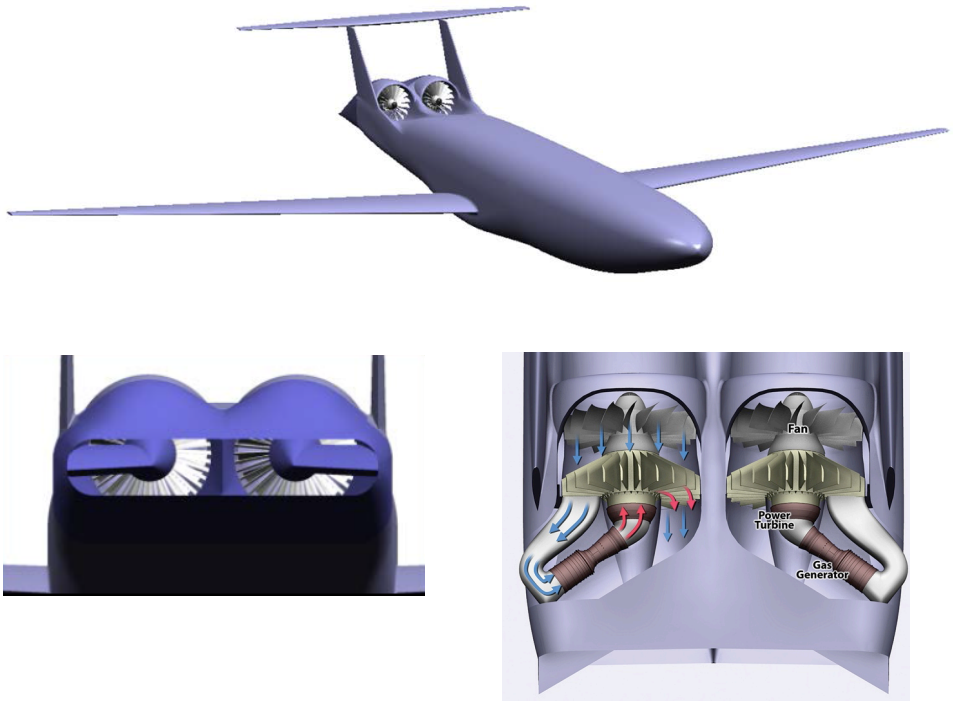

Fig. 27 Unconventional propulsion system architecture for high efficiency small core engine sizes - figure adapted from [48].

acoustics are not - aircraft noise will remain a top concern and unconventional, more integrated installations of the propulsion system will take the acoustic modeling requirements and design space into uncharted territory. The following technologies and their acoustic signature might have to be addressed with innovative and novel modeling approaches.

– Fan and core source noise of advanced propulsion system might become the dominant noise sources. As the fan pressure ratios keep dropping to levels where the blade tip speeds become subsonic, shock noise will be less of a concern and fan broadband noise will become a major challenge. The mitigation of turbomachinery and combustor core noise will yield new challenges due to much reduced engine core sizes and new and innovative architectures. For example, a reversed small core engine, aerodynamically coupled to the propulsor spool might be mounted at an angle with the intake between fan exit guide vanes as the core size is too small to be able to pass the low spool shaft through it. Fig. 27 illustrates the idea for the D8 aircraft with ultra-high bypass ratio engines.

– Dramatically shorter inlets and lighter nacelles will offer less opportunity for acoustic liners so new and innovative concepts for sound attenuation will be needed. Quiet active flow control strategies might be employed both to mitigate source noise and to change the duct impedance. In the limit of the un-shrouded propulsor, or un-ducted counter-rotating fan, blade-passing

tones and blade-row interaction noise will have to be further mitigated to reduce cabin and community noise. New airframe architectures might offer dramatically improved shielding capabilities.

- Boundary layer ingestion and distributed propulsion systems might transform the designs of future aircraft configurations. New propulsion system noise challenges will arise due to more embedded and integrated engine architectures with external and internal flows tightly coupled. New acoustically soft materials, flow control, and mistuned systems might enable system wide noise reductions.

- Electrical machinery noise stemming for example from electric motors and generators, converters and other electrical components will have major impact on the propulsion system acoustic signature. New assessment methods and noise mitigation strategies will have to be employed opening up new research areas in aero-acoustics.

- The growth of small unmanned aerial vehicles for commercial use will have a major impact on community noise and new approaches to noise mitigation and regulation will have to be pursued. Detailed investigations of UAV acoustics are required focussing on how humans and animals perceive and respond to UAV noise. Moreover, new technologies and solutions to mitigating UAV noise governed by close coupled multi-rotor systems will have to be undertaken.

This preliminary list, as incomplete it might be, offers new opportunities for inventions, technologies, and modeling approaches to address the future "grand challenges" in aero-acoustics. These will demand strong collaborations with expert teams cutting across disciplines and bringing academia, industry and government agencies to the same table.

Acknowledgements The work described in this chapter has resulted from contributions of a number of individuals, many of whom are co-authors of the referenced papers. In particular I would like to express my sincere thanks to Dame Ann Dowling at Cambridge University and Edward Greitzer at MIT, the two leads of the Silent Aircraft Project, to James Hileman, my co-Chief Engineer on the project, and to all the students, post-docs, researchers, and industry collaborators involved. The research described in this chapter was funded by the Cambridge-MIT Institute (CMI), NASA Langley Research Center, and the National Institute of Aerospace (NIA). This support is gratefully acknowledged.

****

This chapter is dedicated to my late father Sándor Lajos Ignác Spakovszky who first opened my eyes to the beauty of engineering and ever since instilled in me the passion that comes with it.

References

1. H. Davies: *Airports Commission: Final Report*, July 2015
2. R. Thomas, C. Burley, E. Olson: *Hybrid Wing Body Aircraft System Noise Assessment with Propulsion Airframe Aeroacoustic Experiments*, International Journal of Aeroacoustics vol. 11 (3-4), 2012.
3. A. Manneville, D. Pilczer, Z. Spakovszky: *Preliminary Evaluation of Noise Reduction Approaches for a Functionally Silent Aircraft*, AIAA Journal of Aircraft Vol. 43 No. 3, 2006, pp. 836-840
4. L. Bertsch, W. Heinze, M. Lummer: *Application of an Aircraft Design-To-Noise Simulation Process*, AIAA paper AIAA-2014-2169 (2014)
5. L. Bertsch, F. Wolters, W. Heinze, M. Pott-Pollenske, J. Blinstrub:*System Noise Assessment of a Tube-and-Wing Aircraft with Geared Turbofan Engines*, AIAA paper AIAA-2018-0264 (2018)
6. A. Dowling, E. Greitzer: *The Silent Aircraft Initiative - Overview*, AIAA paper AIAA-2007-0452 (2007)
7. J. Hileman, Z. Spakovszky, M. Drela, M. Sargeant: *Airframe Design for Silent Fuel-Efficient Aircraft*, AIAA Journal Vol. 47, No. 3, May-June 2010

8. Toyota Prius Specifications, Toyota Motor Sales, U.S.A., Torrance, CA, 2005, http://www.toyota.com/prius/specs.html [retrieved Dec. 2006].
9. C. Hall, E. Schwartz, J. Hileman: *Assessment of Technologies for the Silent Aircraft Initiative*, AIAA Journal of Propulsion and Power Vol. 25, No. 6, November-December 2009
10. J. Hileman, T. Reynolds, E. de la Rosa Blanco, T. Law, S. Thomas: *Development of Approach Procedures for Silent Aircraft*, AIAA paper AIAA-2007-0451 (2007)
11. M. Sargeant, T. Hynes, W. Graham, J. Hileman, M. Drela, Z. Spakovszky: *Stability of Hybrid-Wing-Body-Type Aircraft with Centerbody Leading-Edge Carving*, AIAA Journal of Aircraft Vol. 47 No. 3 2010, pp. 970-974
12. M. Herr, W. Dobrzynski: *Experimental Investigations in Low Noise Trailing Edge Design*, AIAA paper AIAA-2004-2804 (2004)
13. A. Quayle, A. Dowling, H. Babinsky, H.-C.Shin, W. Graham, P. Sijtsma: *Landing Gear for a Silent Aircraft*, AIAA paper AIAA-2007-0231 (2007)
14. M. Khorrami, W. Humphreys, D. Lockard, P. Ravetta: *Aeroacoustic Evaluation of Flap and Landing Gear Noise Reduction Concepts*, AIAA paper AIAA-2014-2478 (2014)
15. K. Sakaliyski, J.Hileman, Z. Spakovszky: *Aero-Acoustics of Perforated Drag Plates for Quiet Transport Aircraft*, AIAA paper AIAA-2007-1032 (2007)
16. P. Shah, G. Pfeiffer, R. David, T. Hartley, Z. Spakovszky: *Full-Scale Turbofan Demonstration of a Deployable Engine Air-Brake for Drag Management Appplications*, ASME Turbo Expo Paper GT2016-56708 (2016)
17. M. Drela: *Power Balance in Aerodynamics Flows*, AIAA Journal Vol. 47, No. 7 July 2009
18. T. Law, A. Dowling: *Optimisation of Annular and Cylindrical Liners for Mixed Exhaust Aeroengines*, AIAA paper AIAA 2007-3546 (2007)
19. J. Defoe, Z. Spakovszky: *Effects of Boundary-Layer Ingestion on the Aero-Acoustics of Transonic Fan Rotors*, ASME Journal of Turbomachinery, Vol. 135, September 2013
20. E. de la Rosa Banco, C. Hall, D. Crichton: *Challenges in the Silent Aircraft Engine Design*, AIAA paper AIAA 2007-454 (2007)
21. A. Agarwal, A. Dowling: *Low-Frequency Acoustic Shielding by the Silent Aircraft Airframe*, AIAA Journal Vol. 45 No. 2, 2007, pp. 358-365
22. L. Ng, Z. Spakovszky: *Noise Shielding Assessment of Hybrid Wing-Body Aircraft Configurations*, AIAA Journal, Vo. 49, No. 11, November 2011
23. D. Crichton, E. de la Rosa Blanco, J. Hileman: *Design and Operation for Ultra Low Noise Take-Off*, AIAA paper AIAA-2007-0456 (2007)
24. S. Heath, T. Brooks, F. Hutcheson, M. Doty, C. Bahr, D. Hoad, L. Becker, W. Humphrey, C. Burley, D. Stead, D. Pope, T. Spalt, D. Kuchta, G. Plassman, J. Moen: *NASA Hybrid Wing Aircraft Aeroacoustic Test Documentation Report*, NASA TM-2016-219185 (2016)
25. F. Hutcheson, T. Brooks, C. Burley, C. Bahr, D. Stead, D. Pope: *Shielding of Turbomachinery Broadband Noise by a Hybrid Wing Body Aircraft Configuration*, AIAA paper AIAA-2014-2624 (2014)
26. M. Doty, T. Brooks, C. Burley, C. Bahr, D. Pope: *Jet Noise Shielding Provided by a Hybrid Wing Body Aircraft*, AIAA paper AIAA-2014-2625 (2014)
27. R. Thomas, C. Burley, C. Nickol: *Assessment of the Noise Reduction Potential of Advanced Subsonic Transport Concepts for the NASA Environmentally Responsible Aviation Project*, AIAA paper AIAA-2016-0863 (2016)
28. M. Drela: *Development of the D8 Transport Configuration*, AIAA paper AIAA-2011-3970 (2011)
29. A. Uranga, M. Drela, E. Greitzer, D. Hall, N. Titchener, M. Lieu, N. Siu, C. Casses, A. Huang, G. Gatlin, J. Hannon: *Boundary Layer Ingestion Benefit of the D8 Transport Aircraft*, AIAA Journal, Vol. 55, No. 11, November 2017
30. E. de la Rosa Blanco, J. Hileman: *Noise Assessment of the Double-Bubble Aircraft Configuration*, AIAA paper AIAA-2011-268 (2011)
31. B. Yutko, N. Titchener, C. Courtin, M. Lieu, L. Wirsing, J. Tylko, J. Chambers, T. Roberts, C. Church:*Conceptual Design of a D8 Commercial Aircraft*, AIAA paper AIAA-2017-3590 (2017)
32. L. Lopes, C. Burley: *ANOPP2 User Manual*, NASA TM-2016-219342 (2016)
33. L. Beranek: *Noise and Vibration Control*, NY: McGraw-Hill Book Company, 1971, pp. 174-180
34. Z. Maekawa: *Noise reduction by screens*, Journal of Applied Acoustics, 1968, pp. 157-173
35. D. Nark, C. Burley, A. Tinetti, J. Rawls: *Initial Integration of Noise Prediction Tools for Acoustic Scattering Effects*, AIAA paper AIAA-2008-2996 (2008)
36. D. Colas, Z. Spakovszky: *A Turbomachinery Noise Shielding Framework Based on the Modified Theory of Physical Optics*, AIAA paper AIAA-2013-2136 (2013)
37. D. Colas: *A Diffraction Integral Based Turbomachinery Noise Shielding Method*, Master's Thesis, Department of Aeronautics & Astronautics, MIT, June 2011
38. P. Sunil Kumar, G. Ranganath: *Geometrical theory of diffraction*, J. Phys., 3 (6), pp. 457-488, 1991
39. D. Nark, E. Envia, C. Burley: *Fan Noise Prediction with Applications to Aircraft System Noise Assessment*, AIAA paper AIAA-2009-3291
40. Z. Wang, S. Wu: *Helmholtz Equation Least-Squares Method for Reconstructing the Acoustic Pressure Field*, J. Acoust. Soc. Am., 192(4):2020?2032, October 1997

41. A. Tinetti, M. Dunn: *Aeroacoustic Noise Prediction Using the Fast Scattering Code*, AIAA paper AIAA-2005-3061 (2005)
42. A. Peters, Z. Spakovszky, W. Lord, B. Rose: *Ultrashort Nacelles for Low Fan Pressure Ratio Propulsors*, ASME Journal of Turbomachinery, Vol. 137, February 2015
43. K. Gallagher, S. Goebel, T. Greszler, M. Mathias, W. Oelerich, D. Erogluab, V. Srinivasana: *Quantifying the promise of lithium-air batteries for electric vehicles*, Energy and Environmental Science, 7, 1555 (2014)
44. J. Defoe, A. Narkaj, Z. Spakovszky: *A Body-Force-Based Method for Prediction of Multiple-Pure-Tone Noise: Validation*, AIAA paper AIAA-2010-3747 (2010)
45. G. Podboy, M. Krupar, S. Helland, C. Hughes: *Steady and Unsteady Flow Field Measurements Within a NASA 22 Inch Fan Model*, AIAA paper AIAA-2002-1033 (2002)
46. C. Hughes, R. Jeracki, R. Woodward, C. Miller: *Fan Noise Source Diagnostic Test: Rotor Alone Aerodynamic Performance Results*, AIAA paper AIAA-2002-2426 (2002)
47. J. Defoe, Z. Spakovszky: *Shock Propagation and MPT Noise From a Transonic Rotor in Nonuniform Flow*, ASME Journal of Turbomachinery, Vol. 135, January 2013
48. W. Lord, G. Suciu, K. Hasel, J. Chandler: *Engine Architecture for High Efficiency at Small Core Size*, AIAA paper AIAA-2015-0071 (2015)